



1 The Role of the Size Distribution Shape in Determining Differences
2 between Condensation Rates in Bin and Bulk Microphysics Schemes

3

4 Adele L. Igel¹ and Susan C. van den Heever

5 Department of Atmospheric Science

6 Colorado State University

7 Fort Collins, Colorado

8

9 ¹Corresponding author:

10 1371 Campus Delivery, Fort Collins, CO 80528

11 adele.igel@colostate.edu

12



13 **Abstract.** The condensation rates predicted by bin and bulk microphysics schemes in the same
14 model framework are compared in a novel way using simulations of non-precipitating shallow
15 cumulus clouds. The bulk scheme generally predicts lower condensation rates than does the bin
16 scheme, even when the saturation ratio and the integrated diameter of the droplet size
17 distribution are identical. Despite other fundamental disparities between the bin and bulk
18 condensation parameterizations, the differences in condensation rates are predominantly
19 explained by accounting for the shape of the cloud droplet size distributions simulated by the bin
20 scheme. This shape is not well constrained by observations and thus it is difficult to know how to
21 appropriately specify it in double-moment bulk microphysics schemes. However, this study
22 shows that enhancing our observations may be important since the choice of distribution shape
23 can have a large impact on condensation rates, changing them by 50% or more in some cases.



24 **1. Introduction**

25

26 Bin and double-moment bulk microphysics schemes are both popular approaches for
27 parameterizing subgrid-scale cloud processes (Khain et al., 2015). In double-moment bulk
28 schemes, the mixing ratio and total number concentration for predefined hydrometeor species are
29 typically predicted, and a function is assumed to describe the shape of the size distribution of
30 each species. In contrast, bin schemes do not assume a size distribution function, but instead, the
31 distribution is broken into discrete size bins, and the mixing ratio is predicted for each bin.
32 Usually the size of each bin is fixed, in which case the number concentration is also known for
33 each bin.

34

35 Bin schemes, particularly those for the liquid-phase, are generally thought to describe cloud
36 processes more realistically and accurately than bulk schemes, and thus they are often used as the
37 benchmark simulation when comparing simulations with different microphysics schemes (e.g.
38 Beheng, 1994; Seifert and Beheng, 2001; Morrison and Grabowski, 2007; Milbrandt and Yau,
39 2005; Milbrandt and McTaggart-Cowan, 2010; Kumjian et al., 2012). For the ice phase, bin
40 schemes are plagued by many of the same issues as bulk schemes, such as the use of predefined
41 ice habits and the conversion between ice types, rendering them not necessarily more accurate.
42 Regardless, both liquid- and ice-phase bin schemes are much more computationally expensive
43 since many additional variables need to be predicted. As a result, bin schemes are used less
44 frequently. It is of interest then to see how well bulk and the more accurate liquid-phase bin
45 microphysics schemes compare in terms of predicted process rates, and to assess how much
46 value is added by using a bin instead of a bulk microphysics scheme.



47

48 One of the primary drawbacks of double-moment bulk schemes that assume probability
49 distributions is that many microphysical processes are dependent on the distribution parameters
50 that must be either fixed or diagnosed. In the case of a gamma distribution, this parameter is
51 typically the shape parameter. The gamma size distribution is expressed as

$$52 \quad n(D) = \frac{N}{D_n \nu \Gamma(\nu)} D^{\nu-1} e^{-D/D_n} \quad (1)$$

53 where ν is the shape parameter and all other symbols are defined in Table 1. Much is still to
54 be learned regarding what the most appropriate value of this parameter is, and how it might
55 depend on cloud microphysical properties. Figure 1 shows previously proposed relationships
56 between the cloud droplet number concentration and the shape parameter (Grabowski, 1998;
57 Rotstajn and Liu, 2003; Morrison and Grabowski, 2007; hereinafter G98, RL03, and MG07,
58 respectively) along with values of the shape parameter reported in the literature and summarized
59 by Miles et al. (2000) for several different cloud types. The figure shows a wide range of
60 possible values of the shape parameter based on observations. The lowest reported value is 0.7
61 and the highest is 44.6, though this highest point is clearly an outlier. Furthermore, there is no
62 apparent relationship with the cloud droplet concentration in the data set as a whole, and both
63 increases and decreases of the shape parameter are found with increasing droplet concentration
64 among individual groupings. There is also no clear dependence of the shape parameter on cloud
65 type. Figure 1 also shows that two of the proposed functions relating these two quantities are
66 similar (RL03 and MG07), but that the third function is in total disagreement with these first two
67 (G98).

68



69 Furthermore, using appropriate values of the shape parameter may be necessary for accurately
70 modeling cloud characteristics and responses to increased aerosol concentrations. Morrison and
71 Grabowski (2007) found that switching from the MG07 to the G98 N - v relationships in Fig. 1 led
72 to a 25% increase in cloud water path in polluted stratocumulus clouds. This example shows that
73 inappropriately specifying the shape parameter could have implications for the accurate
74 simulation of not only basic cloud and radiation properties but also for the proper understanding
75 of cloud-aerosol interactions. However, it is apparent from Fig. 1 that *large uncertainties still*
76 *exist regarding the behavior of the shape parameter and how it should be represented in models.*
77 The goal of this study is to compare the condensation and evaporation rates predicted by bin and
78 bulk microphysics schemes in cloud-resolving simulations run using the same dynamical and
79 modeling framework and to assess what the biggest sources of disagreement are. The focus is on
80 condensation and evaporation since these processes occur in all clouds and are fundamental for
81 all hydrometeor species. It will be shown that in spite of other basic differences between the
82 particular bulk and bin microphysics schemes examined here, the lack of a prognosed shape
83 parameter for the cloud droplet size distribution in the bulk scheme is often the primary source of
84 differences between the two schemes, and thus an improved understanding of the shape
85 parameter is necessary from observations and models.

86

87 **2. Condensation/Evaporation Rate Formulations**

88 The Regional Atmospheric Modeling System (RAMS) is used in this study. It contains a double-
89 moment bulk microphysics scheme (RDB) (Saleeby et al., 2004), and the Hebrew University
90 spectral bin model (SBM) (Khain et al., 2004). The SBM is newly implemented in RAMS.
91 Details about the implementation can be found in Appendix A.



92

93 In the RDB microphysics scheme, condensation/evaporation is treated with a bulk approach.

94 Cloud droplet size distributions are assumed to conform to a gamma probability distribution

95 given by Eq. (1). The condensation/evaporation scheme is described in detail in Walko et al.

96 (2000), and the amount of liquid water condensed in a time step is given by their Eq. 6. Here, a

97 slightly rearranged and simplified version of this equation is presented in order to highlight the

98 similarities to the SBM condensation/evaporation equation shown below. Specifically, the RDB

99 condensation/evaporation equation is written as

$$100 \quad r_c^{t+\Delta t} = r_c^* + 2\pi \left[N \bar{D}_v \left(\frac{\Gamma(v)}{\Gamma(v+3)} \right)^{1/3} f_{v,RBE} \right] G_{RBE}(T, r_{vs}, r_c^*) (S^{t+\Delta t} - 1) \Delta t \quad (2)$$

101 By using the value of S at $t+\Delta t$, the full equation for r_v (not shown) is implicit.

102

103 In contrast, the equation for the condensation/evaporation rate in the SBM is given by

$$104 \quad r_c^{t+\Delta t} = r_c^* + 2\pi \left(\sum N_i D_i f_{vi,SBM} \right) G_{SBM}(T, e_s) \int_0^{\Delta t} (S-1) dt \quad (3)$$

105 Semi-analytical equations are used to solve for the time integral of supersaturation that appears at

106 the end of Eq. 3 (Khain and Sednev, 1996).

107

108 Although both equations have the same basic form, there are three primary differences in how

109 these equations are formulated:

- 110 • In the SBM, as is required by the model structure, the condensation rate is calculated for
- 111 each bin of the distribution, and these rates are then summed over all bins, as opposed to
- 112 the integration of the gamma distribution that is done in the RDB scheme.



- 113 • The formulation of the ventilation coefficients and of G_{RDB} and G_{SBM} are different, though
114 the details will not be discussed here.
- 115 • The time step integration is performed semi-analytically in the SBM with multiple sub-
116 time steps rather than implicitly in the RDB scheme.

117 These differences between the bin and bulk schemes will be taken into consideration in this
118 analysis in order to understand why the two schemes produce different condensation rates.

119

120 **3. Simulations**

121 In order to investigate the difference in condensation rates predicted by the two microphysics
122 schemes, simulations of *non-precipitating* shallow cumulus clouds over land were performed.
123 This cloud type was chosen in order to minimize the indirect impacts of precipitation processes
124 and thus facilitated the direct comparison of condensation rates. Furthermore, the daytime
125 heating and evolution of the boundary layer results in a wider range of thermodynamic
126 conditions than would occur in simulations of maritime clouds. The wider range of
127 thermodynamic conditions make the conclusions of this study more robust. The simulations were
128 run with RAMS and employed 50m horizontal spacing and 25m vertical spacing over a grid that
129 is 12.8 x 12.8 x 3.5 km in size. The simulations are run for 9.5 hours (after this time the clouds
130 hit the model top) using a 1s time step. The simplified profiles of potential temperature,
131 horizontal wind speed, and water vapor mixing ratio based on an ARM SGP sounding from 6
132 July 1997 at 1130 UTC (630 LST) presented in Zhu and Albrecht (2003) (see their Fig. 3) are
133 used to initialize the model horizontally homogeneously. The initial profiles of potential
134 temperature and relative humidity are reproduced in Fig. 2. The wind direction is taken to be 0°
135 throughout the domain. Random temperature and moisture perturbations are applied to the



136 lowest model level at the initial time. The Harrington (1997) radiation scheme is used for
137 simulations with both microphysics parameterizations. Surface fluxes were predicted using the
138 LEAF-3 land surface model (Walko et al., 2000) and a short grass vegetation type was assumed.

139

140 Some modifications were made to the model for this study only in order to make the two
141 microphysics schemes more directly comparable. The calculation of relative humidity was
142 changed in the RDB scheme to make it the same as the calculation in the SBM. The SBM does
143 not include a parameterization for aerosol surface deposition, so this process was turned off in
144 the RDB scheme. Finally, the regeneration of aerosol upon droplet evaporation was deactivated
145 in both microphysics schemes. Aerosol concentrations were initialized horizontally and
146 vertically homogeneously. Aerosol particles did not interact with radiation.

147

148 Three simulations were run with the RDB scheme and three with the SBM scheme. Since the
149 relationships in Fig. 1 (G98; RL03; MG07) suggest that the shape parameter may depend on the
150 cloud droplet number concentration, the simulations were run with three different aerosol
151 concentrations, specifically, 100, 400, and 1600 cm⁻³, in order to obtain a larger range of droplet
152 concentration values. The number concentration of 100 cm⁻³ is somewhat uncommon over land,
153 but it is necessary to use this value in order to explore more fully the range of possible
154 microphysical conditions. The simulations will be referred to by the microphysics scheme
155 abbreviation and the initial aerosol concentration, e.g. SBM100 and RDB1600.

156

157 **4. Results**

158 **4.1 Instantaneous Condensation Rates**



159 In order to compare directly the condensation rates predicted by the RDB and SBM microphysics
160 schemes, it is necessary to evaluate these rates given the same thermodynamic and cloud
161 microphysical conditions. The RDB condensation equation (Eq. (2)) is approximately
162 proportional to four quantities: S , N , \bar{D} , and v . We say approximately proportional since the
163 presence of the ventilation coefficient and the time-stepping methods make these factors not
164 truly proportional to the condensation rate. In the SBM scheme, the condensation rate is only
165 explicitly proportional to S , and the SBM scheme does not make assumptions about the
166 functional form of the size distribution. If it is assumed nevertheless that the SBM size
167 distributions can be described by some probability distribution function (which doesn't
168 necessarily have to be a gamma distribution), then Eq. (3) could also be rewritten to be
169 approximately proportional to N and \bar{D} . Therefore, in order to compare best the condensation
170 rates between the two schemes, the condensation and evaporation rates that occur during one
171 time step were binned by the values of S and $N\bar{D}$ (hereafter referred to as the integrated
172 diameter) that existed at the start of the condensation/evaporation process and were averaged in
173 each bin. Where the cloud was supersaturated and subsaturated, saturation ratio bin widths of 0.1
174 and 1 were used, respectively. For $N\bar{D}$, bin widths of 0.05 m g^{-1} were used. The output from the
175 model only includes the values of S , N , and \bar{D} after condensation and evaporation have occurred.
176 However, since the rates of condensation and droplet nucleation were known, and since
177 microphysics is the last physical process to occur during a time step in RAMS, the S , N and \bar{D}
178 that existed before condensation occurred were easily obtained. All points where the cloud
179 mixing ratio before condensation was greater than 0.01 g kg^{-1} are included in the analysis.
180



181 Note that the aerosol activation parameterizations in the RDB and SBM microphysics are not the
182 same, and hence the number of nucleated cloud droplets is not the same. This will impact the
183 frequency at which each joint S and $N\bar{D}$ bin occurs. However, we are primarily concerned with
184 the average condensation rate in each joint bin, and the average value will not be impacted by the
185 aerosol activation parameterizations since we are explicitly accounting for differences in the
186 number and size of droplets through the use of $N\bar{D}$ in our analysis. Therefore the differences in
187 the aerosol activation parameterizations should not influence the differences in the average
188 condensation rates as evaluated in our framework.

189

190 The average condensation rate in each S and $N\bar{D}$ bin was calculated for all simulations. Figure 3
191 shows an example of this calculation for one simulation. As is seen in Fig. 3, there is a smooth
192 transition to higher condensation rates as the saturation ratio increases, and to higher
193 condensation ($S \geq 1$) and evaporation ($S < 1$) rates as the integrated diameter increases. This is
194 expected based on the condensation equations (Eqs. (2), (3)). All other simulations behave
195 similarly.

196

197 In order to compare easily the condensation rates predicted by the two microphysics schemes,
198 Fig. 4a-c shows the ratio of the RDB to SBM condensation rates in the S and $N\bar{D}$ phase space. It
199 reveals that for low integrated diameter values, the RDB scheme predicts higher condensation
200 rates, but that almost everywhere else, the condensation rate is higher in the SBM scheme
201 simulations. In the RDB1600 and SBM1600 simulations, the RDB scheme predicts lower
202 condensation rates almost everywhere. In all cases, the ratios are lowest (RDB rates are lower
203 than SBM rates) where $N\bar{D}$ is large.



204

205 For evaporation (Fig. 3d-f), the RDB and SBM rates are more similar than for condensation. The
206 disagreement is worst for very low relative humidity values, very low integrated diameter values,
207 as well as for moderate values of both quantities. In all of these cases, the difference is 25% or
208 more. However, where evaporation occurs most frequently (at high saturation ratio and low
209 integrated diameter; not shown), the differences are generally less than 10%. Thus it appears that
210 the evaporation rates between the two schemes generally agree better than do the condensation
211 rates.

212

213 There are many potential reasons why the condensation and evaporation rates are different
214 between the two schemes. As the following analysis will show, one major source of discrepancy
215 is that the cloud droplet size distribution assumed by the RDB scheme is not always
216 representative of what the SBM scheme simulates.

217

218 **4.2 Shape Parameter**

219 As can be seen in the condensation equation for the RDB scheme (Eq. 2), when a gamma
220 distribution is assumed, the condensation rate is proportional to the shape parameter ν such that a
221 higher shape parameter results in higher condensation rates. The SBM scheme makes no
222 assumptions about the size distribution shape. However, in order to characterize the predicted
223 SBM size distributions, and to facilitate the comparison of the SBM and RDB condensation
224 rates, we assume that the predicted SBM size distributions are gamma distribution-like and find
225 the best-fit gamma distribution parameters (see Eq. (1)) for the cloud droplet size distributions at
226 every cloudy grid point in the SBM simulations. We then evaluate the mean best-fit shape



227 parameter for each point in the S and $N\bar{D}$ phase space. These best-fit shape parameters are then
228 used to assess whether the assumption of a constant shape parameter could explain differences
229 between the RDB and SBM average condensation rates

230

231 In order to find the best-fit shape parameters, we define cloud droplets as belonging to one of the
232 first 15 bins of the SBM liquid array, which corresponds to a maximum cloud droplet diameter
233 of 50.8 μm . Many methods are available to find such best-fit parameters, but they generally all
234 give similar results (McFarquhar et al., 2014). Here we use the maximum-likelihood estimation
235 method and find best-fits that minimize the error in the total number concentration. Using this
236 method, the size distributions are first normalized by the corresponding total number
237 concentration, leaving only D_n and v as free parameters of the distribution (Eq. 1).

238

239 Note that while we could determine the values of S and $N\bar{D}$ that existed before condensation
240 occurred, we cannot determine the value of the best-fit shape parameter for this time because the
241 change in mixing ratio of each bin is not output by RAMS. Thus the average shape parameters
242 used in the analysis are those that exist at the end of the time step. Nonetheless, given the short
243 time step used in these simulations, it is not expected that the best-fit shape parameter would
244 change much in one time step and thus the impact of using the post-condensation shape
245 parameters is not expected to have a large impact on the results.

246

247 Figure 5 displays a scatterplot of the average shape parameters and the condensation and
248 evaporation rate ratios presented in Fig. 4 for each of the three sets of simulations. The black line
249 plotted in all three panels is the same and shows the theoretical condensation rate ratio that we



250 would expect if there were no other differences between the bin and bulk condensation equations
251 aside from the value of the shape parameter (and assuming that the bin scheme always predicts
252 cloud droplet size distributions that conform to a gamma distribution). Recall that in the RDB
253 simulations the shape parameter is constant and has a value of 4. Therefore, specifically, the line

254 is equal to $4 \left(\frac{\Gamma(4)}{\Gamma(7)} \right)^{1/3} / \nu \left(\frac{\Gamma(\nu)}{\Gamma(\nu+3)} \right)^{1/3}$ (see the ν dependency in Eq. 2).

255

256 In all three pairs of simulations, the mean shape parameter in the SBM simulations explains a
257 large fraction of the variability in the condensation rate ratios, particularly for points with a
258 supersaturation greater than 0.1% (blue dots) or a relative humidity between 90 and 99% (yellow
259 dots). Note that at low shape parameter values, both the theoretical ratio and the modeled ratios
260 indicate that the RDB prediction can be 50% higher than the SBM prediction or more. As the
261 initial aerosol concentration increases, the spread of the points in these two categories around the
262 theoretical expectation increases but is otherwise qualitatively similar. The increased spread is in
263 part due to the fact that the RDB1600 and SBM1600 simulations cover a larger area of the S and
264 $N\bar{D}$ phase space (Fig. 4). Therefore there are more points displayed in Fig. 5c and each point has
265 on average fewer instances of condensation included in its average (not shown). As a result, it is
266 difficult to draw conclusions about how the bulk versus bin condensation rates change as a
267 function of the initial aerosol concentration, except to say that aside from the change in spread,
268 there are no startling differences.

269

270 The quality of the match between the predicted and the model-derived condensation ratios is
271 lower for points with relative humidity values close to saturation (99-100.1%; orange dots).



272 These points tend to lie much farther from the predicted ratio line and show less correlation with
273 the mean shape parameter value. Many points in this category instead have ratios near 1,
274 indicating that both schemes predict the same condensation/evaporation rates. For these points, it
275 is likely that the supersaturation or subsaturation is entirely removed in one time step. In such a
276 case, the shape of the droplet size distribution, as well as all of the other scheme differences, has
277 no impact on the condensation/evaporation rate. If, on the other hand, the supersaturation or
278 subsaturation is nearly, but not entirely removed, the predicted rate is likely sensitive to the
279 scheme's time stepping method and large differences between the condensation/evaporation rates
280 predicted by the two schemes can arise. Finally, at high sub-saturation (0-89% RH; purple dots),
281 the ability of the shape parameter to predict the condensation rate ratio is also diminished. In this
282 regime, cloud water mixing ratio is low and droplets are small. Any of the other differences
283 between the two condensation schemes could be responsible for the disagreement here.

284

285 **5. Discussion and Conclusions**

286 In this study we have conducted a comparison of the condensation rates predicted by a bulk and
287 a bin microphysics scheme in simulations of non-precipitating cumulus clouds run using the
288 same dynamical framework, namely RAMS. The simulations were run with three different
289 background aerosol concentrations in order to consider a large range of microphysical
290 conditions. When the condensation rates were binned by saturation ratio and integrated diameter,
291 the RDB rates were on average higher only for evaporation at low relative humidities and for
292 condensation at low integrated diameter values. Otherwise, the RDB condensation and
293 evaporation rates were consistently lower than those predicted by the SBM. Further analysis
294 indicated that the fixed shape parameter assumed for RDB cloud droplet size distributions



295 explained much of the discrepancy in condensation rates between the two schemes, particularly
296 when the supersaturation was greater than 0.1% or the relative humidity was 90-99%. For
297 relative humidity values close to 100% (99-100.1%), the two schemes often predicted similar
298 rates regardless of the best-fit shape parameter values from the SBM. A number of conclusions
299 can be drawn from these results:

- 300 1. A gamma probability distribution appears to be a good assumption for the cloud droplet
301 distribution shape, and the exact knowledge of the distribution shape in a bin scheme is
302 often not necessary to minimize errors in the condensation rate in bulk schemes.
- 303 2. Given that the shape parameter associated with the bin scheme cloud distributions
304 explains the condensation rate ratios well under most conditions, differences in the
305 formulations of the ventilation coefficient and G terms may not be important except
306 possibly when the relative humidity is low.
- 307 3. For relative humidity conditions near saturation, the rates predicted by bin and bulk
308 schemes are often similar since the supersaturation or subsaturation is entirely consumed
309 in one time step. If, on the other hand, the supersaturation or subsaturation is only mostly
310 removed, then large discrepancies in the condensation rates may appear.
- 311 4. Except when small residual supersaturation or subsaturation remains at the end of the
312 model time step, the multiple sub-time steps taken by the SBM scheme may not strongly
313 impact the total amount of condensed water in the full time-step and thus it may not be
314 necessary to use such computationally expensive methods.

315 In conclusion, it appears that *the most important factor for agreement in cloud droplet*
316 *condensation rates between bin and bulk schemes is the shape of the cloud droplet size*



317 *distribution*. And while we have not explicitly explored them here, we would expect this basic
318 conclusion to hold for other hydrometeor types as well.

319

320 We have presented here a novel method for comparing condensation rates between any two
321 microphysics schemes. Although we have only investigated two specific schemes, it is expected
322 that the results can be applied more generally to bulk and bin schemes. Additional work should
323 be conducted using a similar approach in order to compare and evaluate additional microphysics
324 schemes and additional microphysical processes. While it is clear that the effective shape
325 parameter in the bin simulations explains much of the discrepancies in predicted condensation
326 rates between bin and bulk schemes, and that the shape parameter value can change the
327 condensation rate by 50% or more, our understanding of what the most appropriate value of the
328 shape parameter is or how it should vary as a function of basic cloud properties is limited. More
329 work then is also needed on understanding cloud droplet distributions from observations and
330 measurements.

331

332 **Acknowledgements:**

333 The authors thank Alexander Khain for generously sharing his SBM code in order to make this
334 study possible. This material is based on work supported by the National Science Foundation
335 Graduate Research Fellowship Program under Grant No. DGE-1321845 and the National
336 Aeronautics and Space Administration Grant No. NNX13AQ32G. Additional information can be
337 found in the supporting information or be requested from the corresponding author.

338

339 **Appendix A**



340 **Implementation of the Hebrew University SBM scheme into RAMS**

341

342 While the present study is only concerned with warm phase processes, the methods to interface
343 the Hebrew University SBM scheme with the RAMS radiation scheme (Harrington, 1997) will
344 be described here, including those for the ice species. The RAMS radiation scheme uses pre-
345 computed lookup tables for the extinction coefficient, single-scattering albedo, and asymmetry
346 parameter for each hydrometeor species. Three of the hydrometeor species in the SBM
347 correspond directly to species in the RAMS microphysics scheme, namely, aggregates, graupel,
348 and hail. All liquid drops are represented as one species in the SBM, so these liquid bins are
349 classified as either cloud droplets or rain drops using the same size threshold used by the RAMS
350 microphysics scheme to distinguish these two species. Finally, the SBM represents three ice
351 crystal types – plates, columns, and dendrites. Separate RAMS radiation look-up tables already
352 exist for these different ice crystal types, but like for cloud and rain, there are two tables for each
353 crystal type depending on the mean size of the crystals. In RAMS, the small ice crystals are
354 referred to as pristine ice, and the large ice crystals as snow. Again, the same size threshold used
355 to distinguish these two ice categories is used to assign bins from the SBM ice crystal species as
356 either pristine ice or snow. This fortuitous overlap in the ice species has allowed for the
357 seamless integration of the SBM hydrometeor species with the RAMS radiation scheme. For
358 each set of SBM bins that corresponds to a RAMS species, the total number concentration and
359 mean diameter is calculated, a gamma distribution shape parameter of 2 is assumed, and the
360 appropriate set of look-up tables for the corresponding RAMS species is used for all radiative
361 calculations.

362



363 **References:**

- 364 Beheng, K. D.: A parameterization of warm cloud microphysical conversion processes,
365 Atmos. Res., 33, 193–206, doi:10.1016/0169-8095(94)90020-5, 1994.
366
- 367 Grabowski, W. W.: Toward Cloud Resolving Modeling of Large-Scale Tropical Circulations:
368 A Simple Cloud Microphysics Parameterization, J. Atmos. Sci., 55(21), 3283–3298,
369 doi:10.1175/1520-0469(1998)055<3283:TCRMOL>2.0.CO;2, 1998.
370
- 371 Harrington, J. Y.: The effects of radiative and microphysical processes on simulation of
372 warm and transition season Arctic stratus, Colorado State University., 1997.
373
- 374 Khain, A., Pokrovsky, A., Pinsky, M., Seifert, A. and Phillips, V.: Simulation of Effects of
375 Atmospheric Aerosols on Deep Turbulent Convective Clouds Using a Spectral Microphysics
376 Mixed-Phase Cumulus Cloud Model. Part I: Model Description and Possible Applications, J.
377 Atmos. Sci., 61(24), 2963–2982, doi:10.1175/JAS-3350.1, 2004.
378
- 379 Khain, A. P. and Sednev, I.: Simulation of precipitation formation in the Eastern
380 Mediterranean coastal zone using a spectral microphysics cloud ensemble model, Atmos.
381 Res., 43(1), 77–110, doi:10.1016/S0169-8095(96)00005-1, 1996.
382
- 383 Khain, A. P., Beheng, K. D., Heymsfield, A., Korolev, A., Krichak, S. O., Levin, Z., Pinsky, M.,
384 Phillips, V., Prabhakaran, T., Teller, A., van den Heever, S. C. and Yano, J.-I.: Representation
385 of microphysical processes in cloud-resolving models: Spectral (bin) microphysics versus



386 bulk parameterization, Rev. Geophys., 53(2), 247–322, doi:10.1002/2014RG000468, 2015.

387

388 Kumjian, M. R., Ganson, S. M. and Ryzhkov, A. V.: Freezing of Raindrops in Deep Convective

389 Updrafts: A Microphysical and Polarimetric Model, J. Atmos. Sci., 69(12), 3471–3490,

390 doi:10.1175/JAS-D-12-067.1, 2012.

391

392 McFarquhar, G. M., Hsieh, T.-L., Freer, M., Mascio, J. and Jewett, B. F.: The Characterization of

393 Ice Hydrometeor Gamma Size Distributions as Volumes in $N_0 - \lambda - \mu$ Phase Space:

394 Implications for Microphysical Process Modeling, J. Atmos. Sci., 72(2), 892–909,

395 doi:10.1175/JAS-D-14-0011.1, 2015.

396

397 Milbrandt, J. A. and McTaggart-Cowan, R.: Sedimentation-Induced Errors in Bulk

398 Microphysics Schemes, J. Atmos. Sci., 67(12), 3931–3948, doi:10.1175/2010JAS3541.1,

399 2010.

400

401 Milbrandt, J. A. and Yau, M. K.: A Multimoment Bulk Microphysics Parameterization. Part I:

402 Analysis of the Role of the Spectral Shape Parameter, J. Atmos. Sci., 62(9), 3051–3064,

403 doi:10.1175/JAS3534.1, 2005.

404

405 Miles, N. L., Verlinde, J. and Clothiaux, E. E.: Cloud Droplet Size Distributions in Low-Level

406 Stratiform Clouds, J. Atmos. Sci., 57(2), 295–311, doi:10.1175/1520-

407 0469(2000)057<0295:CDS DIL>2.0.CO;2, 2000.

408



- 409 Morrison, H. and Grabowski, W. W.: Comparison of Bulk and Bin Warm-Rain Microphysics
410 Models Using a Kinematic Framework, *J. Atmos. Sci.*, 64(8), 2839–2861,
411 doi:10.1175/JAS3980, 2007.
- 412
- 413 Rotstayn, L. D. and Liu, Y.: Sensitivity of the First Indirect Aerosol Effect to an Increase of
414 Cloud Droplet Spectral Dispersion with Droplet Number Concentration, *J. Clim.*, 16(21),
415 3476–3481, doi:10.1175/1520-0442(2003)016<3476:SOTFIA>2.0.CO;2, 2003.
- 416
- 417 Saleeby, S. M. and Cotton, W. R.: A Large-Droplet Mode and Prognostic Number
418 Concentration of Cloud Droplets in the Colorado State University Regional Atmospheric
419 Modeling System (RAMS). Part I: Module Descriptions and Supercell Test Simulations, *J.*
420 *Appl. Meteorol.*, 43(1), 182–195, doi:10.1175/1520-
421 0450(2004)043<0182:ALMAPN>2.0.CO;2, 2004.
- 422
- 423 Saleeby, S. M. and van den Heever, S. C.: Developments in the CSU-RAMS Aerosol Model:
424 Emissions, Nucleation, Regeneration, Deposition, and Radiation, *J. Appl. Meteorol. Climatol.*,
425 52(12), 2601–2622, doi:10.1175/JAMC-D-12-0312.1, 2013.
- 426
- 427 Seifert, A. and Beheng, K. D.: A double-moment parameterization for simulating
428 autoconversion, accretion and selfcollection, *Atmos. Res.*, 59-60, 265–281,
429 doi:10.1016/S0169-8095(01)00126-0, 2001.
- 430
- 431 Walko, R. L., Band, L. E., Baron, J., Kittel, T. G. F., Lammers, R., Lee, T. J., Ojima, D., Pielke, R.

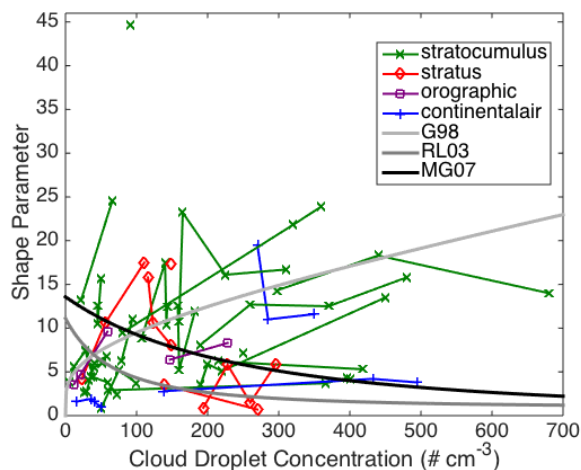


- 432 A., Taylor, C., Tague, C., Tremback, C. J. and Vidale, P. L.: Coupled atmosphere, biophysics
 433 and hydrology models for environmental modeling, J. Appl. Meteorol., 39, 931–944,
 434 doi:10.1175/1520-0450(2000)039<0931:CABHMF>2.0.CO;2, 2000a.
 435
- 436 Walko, R. L., Cotton, W. R., Feingold, G. and Stevens, B.: Efficient computation of vapor and
 437 heat diffusion between hydrometeors in a numerical model, Atmos. Res., 53(1-3), 171–183,
 438 doi:10.1016/S0169-8095(99)00044-7, 2000b.
 439
- 440 Zhu, P. and Albrecht, B.: Large eddy simulations of continental shallow cumulus convection,
 441 J. Geophys. Res., 108(D15), 4453, doi:10.1029/2002JD003119, 2003.
 442
- 443 Table 1. Definitions of symbols used.

Symbol	Definition
e_s	Saturation water vapor pressure
D	Cloud droplet diameter
\bar{D}	Volume mean cloud droplet diameter. $r_c = \pi \rho_w \bar{D}^3 / 6$
D_n	Characteristic cloud droplet diameter. $D_n^3 = \bar{D}^3 \Gamma(v) / \Gamma(v+3)$
$f_{v,RDB}, f_{v,SBM}$	Ventilation coefficients for the RDB and SBM schemes, respectively
G_{RDB}, G_{SBM}	Term to account of the impact of latent heat release on the condensation process. See <i>Walko et al.</i> [2000] and <i>Khain and Sednev</i> [1996] for the formulations used in the RDB and SBM schemes, respectively
N	Cloud droplet number concentration
n	Concentration of cloud droplets per unit cloud droplet diameter interval
r_c	Cloud water mixing ratio
r_v	Water vapor mixing ratio
r_{vs}	Saturated water vapor mixing ratio
S	Saturation ratio
T	Air temperature
t	Time
Γ	Gamma function
v	Gamma distribution shape parameter
$()^*$	Value of a quantity after advection and all other model processes but before microphysical processes have occurred during a model time step

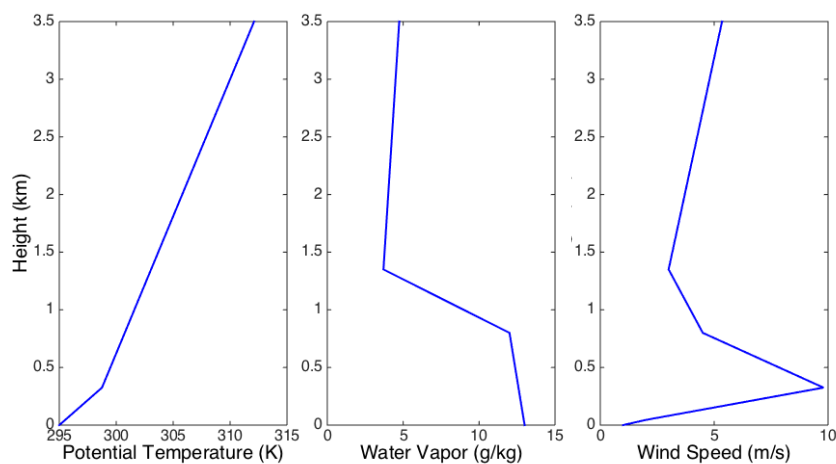


444



445

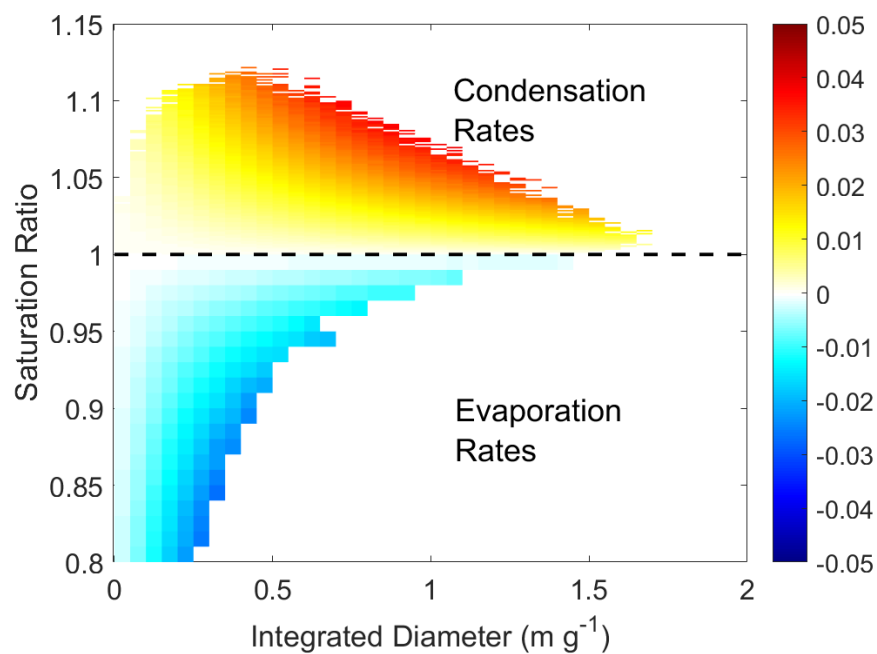
446 Figure 1. Shape parameter (ν) values as a function of cloud droplet concentration as
447 reported by Miles et al. (2000) using 16 previous studies. Values, cloud classification, and
448 groupings are based on their Tables 1 and 2. The three solid gray lines show proposed
449 relationships between the cloud droplet concentration and the shape parameter. G98 is
450 from Eq. 9 in Grabowski (1998). RL03 is from Eq. 3 in Rotstajn and Liu (2003) with their
451 $\alpha=0.003$. MG07 is from Eq. 2 in Morrison and Grabowski (2007). All equations were
452 originally written for relative dispersion, which is equal to $\nu^{-1/2}$, and have been converted to
453 equations for ν for this figure.



454

455 Figure 2. Profiles of potential temperature, water vapor, and wind speed used to initialize the
456 simulations from Zhu and Albrecht (2003).

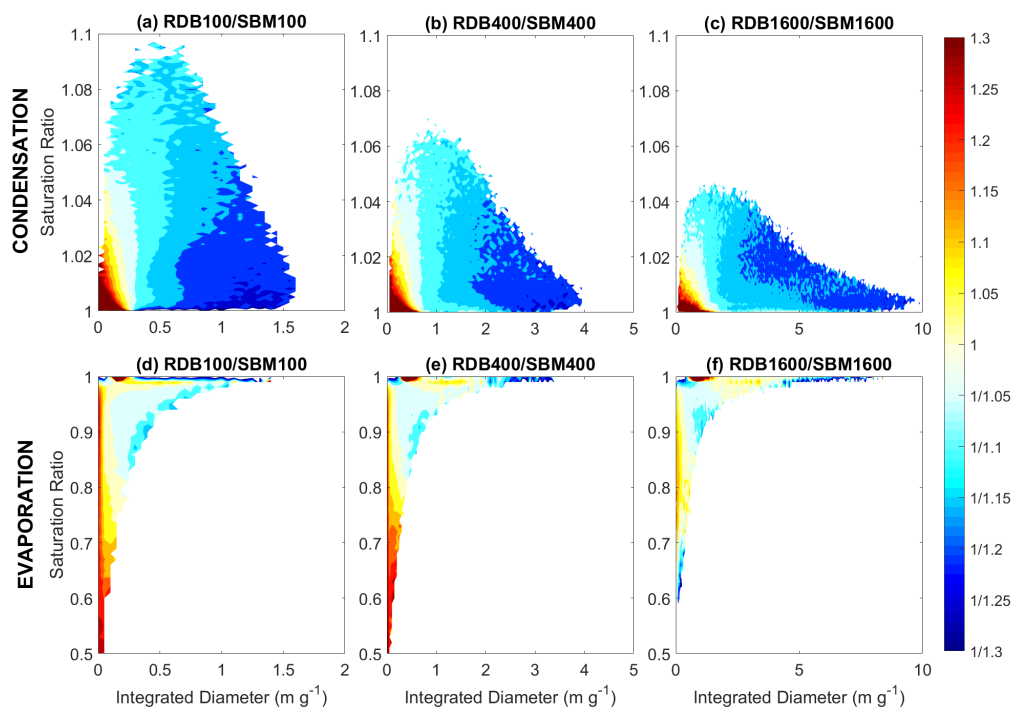
457



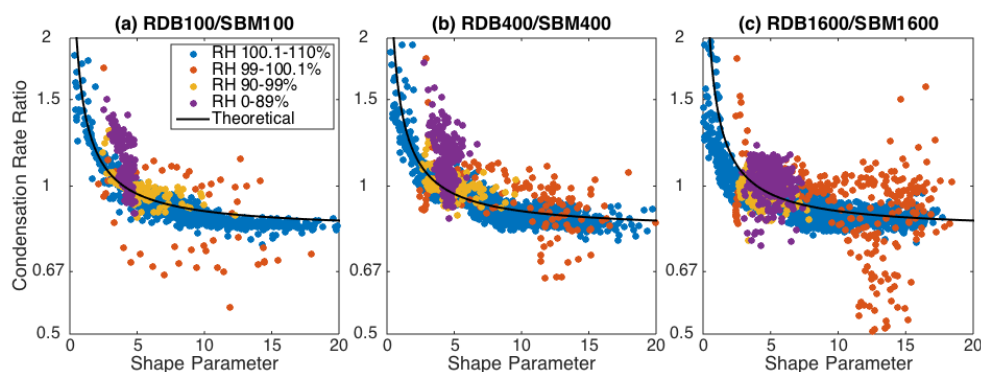
458



459 Figure 3. The average condensation and evaporation rates ($\text{g kg}^{-1} \text{s}^{-1}$) as a function of
460 saturation ratio (S) and integrated diameter ($N\bar{D}$) for the SBM100 simulation.
461



462
463 Figure 4. The ratio of the RDB to SBM (a-c) condensation and (d-f) evaporation rates as a
464 function of saturation ratio (S) and integrated diameter ($N\bar{D}$) for each pair of simulations.
465 Note the differences in axes limits.



466

467 Figure 5. Scatterplots of the condensation rate ratios (RDB/SBM) and mean best-fit shape
468 parameters from the SBM simulations. Each point shows values from a joint bin in the S
469 and $N\bar{D}$ phase space in Figure 3. The black line is identical in all three plots and displays the
470 theoretical condensation rate ratio obtained by assuming that no other differences exist
471 between the two schemes aside from the value of the best-fit shape parameter. See the text
472 for more details.